Supplementary Material for:

Autosomal Recessive Progeroid Syndrome due to Homozygosity for a *TOMM7* Variant

Supplemental Data Table of Contents

List of Investigators:

Abhimanyu Garg, MD, Wee-Teik Keng, MBBS, MRCP, Zhenkang Chen, PhD, Adwait Amod Sathe, PhD, Chao Xing, PhD, Pavithira Devi Kailasam, MBBS, Yanqiu Shao, MS, Nicholas P. Lesner, PhD, Claire B. Llamas, BS, Anil K. Agarwal, PhD, Prashant Mishra, MD, PhD

Methods:

Genome sequencing and analysis:

Genomic DNA was isolated from peripheral blood using the Easy-DNA kit (Invitrogen, Carlsbad, CA). The proband, his two unaffected siblings, and their parents underwent whole exome sequencing using the Integrated DNA Technologies xGen Exome Research Panel V.1.0 on the Illumina platform. The mean coverage of the targeted regions was >100-fold with > 95% of bases covered by >50-fold reads in all samples. Additionally, the proband underwent whole genome sequencing with the mean coverage of 107-fold and 97% of bases covered by >50-fold reads. Sequencing read length was paired-end 2x150 bp in both experiments. Sequences were aligned to the human reference genome b37, and variants were called using the Genome Analysis Toolkit (v3.8) (1) and annotated using SnpEff (v5.1) (2).

We hypothesized an autosomal recessive inheritance and searched for homozygous or compound heterozygous disease-causing variants. Therefore, we filtered for rare missense, nonsense, splicing, or frame shift variants either homozygous or compound heterozygous in the proband but not in the two unaffected siblings or their parents. Other criteria included the minor allele frequency (MAF) less than 0.01 in the 1000 Genomes Project (http://www.internationalgenome.org/) and genome aggregation database (gnomAD; http://gnomad.broadinstitute.org/), the Genomic Evolutionary Rate Profiling (GERP)++ score (3) greater than 2.0, and the Combined Annotation Dependent Depletion (CADD) score (4) greater than 15. We also identified runs of homozygosity (ROH) in the proband but not shared by the unaffected parents and siblings using BCFtools/RoH (v1.9) (5). The ROH regions were further screened for rare non-coding variants in the WGS data of the proband. Sanger sequencing was preformed to confirm the co-segregation of the candidate variant with the phenotype in the pedigree. Besides, de novo mutation detection, CNVkit (v.0.9.9) (6), and Manta (v1.3) (7) were

run to detect mutations, copy number variations, and structure variations present in the proband but not in the other four unaffected family members.

CRISPR-editing of mouse embryos:

A sgRNA targeting the mouse *Tomm7* locus was co-injected into C57BL/6 mouse zygotes with single-stranded DNA containing the P29L variant (Figure S6A), and then implanted into pseudo-pregnant females. sgRNA and ssDNA species were synthesized by Integrated DNA Technologies (Coralville, IA). F0 mice were genotyped using locus-specific primers: mmTomm7_fw1 CACGACTCCTGCCGTAAAG and mmTomm7_rv1 AGGGATTGTGTGCTGGTTAAA to amplify a PCR-product surrounding the P29L mutation, followed by Sanger sequencing. Founder animals were back-crossed to C57BL/6 animals for three generations. Homozygous P29L/P29L animals were obtained by P29L/+ x P29L/+ crosses, and verified by Sanger sequencing.

Cell Culture:

Unaffected human fibroblasts, control # 2,3,4,5 were obtained from Coriell Institute for Medical Research (Camden, NJ) or from a normal volunteer (N300). The proband's fibroblasts (MAD5700.25) were established at the core laboratory at UTSW. All fibroblast cells were grown in Minimum essential medium (MEM) supplemented with antibiotic–antimycotic and 15% fetal bovine serum. Cell cultures were maintained in a humidified incubator at 37°C in 5% CO_2. HEK293 and HeLa cells were obtained from ATCC.

To obtains *Tomm7*$^{-/-}$ HeLa cells, a sgRNA targeting exon 1 of the Tomm7 locus (sequence below) was cloned into the *BbsI* site of plasmid PX458 (Addgene 48138). HeLa cells were transfected with 2ug of PX458 plasmids, and GFP-positive single cells were sorted at 48 hour post-transfection using a FACS Aria SORP. After single colonies were obtained, clones were screened by Western blot for loss of TOMM7 protein. To verify genomic editing, the portion of the

TOMM7 locus was amplified (primer sequences below), followed by cloning and sequencing using the pGEM-T vector system (Promega, A1360).

hsTomm7 sgRNA: GGAGCAGTGAACCCGCAAGG

hsTomm7_seqforward primer: CCTCCTTTCCCTTTCGGATTC

hsTomm7_seqreverse primer: TGACCTCCACTTTAAGGATGC

Primary mouse fibroblasts were isolated from tails of 2 week old mice using established protocols (8). Briefly, tails were washed with 70% EtOH, air-dried, and cut into small pieces (~3mm in size). The tissue was incubated in DMEM supplemented with 1mg/mL collagenase and dispase (Sigma) at 37°C for 90 minutes. The solution was grinded through a 70 μm cell strainer into 10 cm dishes containing 10 mL of complete media. The cell suspension was collected into a 15 mL conical tube and spun down at 300xg. The pellet was resuspended in 10mL complete medium + 20 μL amphotericin B solution (Thermo Fisher, R01510), and plated in a fresh 10cm dish. Cells were incubated at 37°C for 3-4 days to allow fibroblasts to grow out. Cell debris was then washed away, and cells were trypsinized and replated following standard cell culture methods.

DNA extraction:

DNA was extracted from fibroblast cells using two different methods. First, for confirmation of the *Tomm7* variant, genomic DNA was extracted using an Invitrogen EasyDNA kit (cat # 45-0424, Invitrogen; lot #2209814) following the manufacturer's protocol. In brief, fibroblast cells were scraped from the dishes and added to the QuickExtract solution and vortexed for 15 seconds. The solution was incubated at 65°C for 15 minutes and vortexed for 15 seconds. The tube was incubated at 98°C for 2 minutes and the DNA stored at -20°C overnight. Confirmation of the *TOMM7* variant at the genomic level was carried out using genomic DNA extracted from the

fibroblasts using the flanking primers (as shown below) to amplify the desired genomic region. The PCR product was gel confirmed and sequenced.

TOMM7_rs778567973_F 5'-CTCACGACTCCTGCCGTAA-3'

TOMM7_rs778567973_R 5'- GAACGGGAACTCGAACTCAG

RNA isolation:

We employed a general method routinely used for total RNA extraction (RNA STAT-60; Tel-Test, Friendswood, TX) and RT-qPCR.(9) Similarly, the RNA was reverse transcribed(9) and the cDNA was amplified and sequenced using primer pair shown below, using a touchdown PCR reaction protocol.(10)

hTOMM7 RNA F 5'-ATTCCCGACGCTGTGGTT-3'

hTOMM7 RNA R 5'-CAGATGCGTCTGTGAAGAGC-3'

Mitochondria labeling and Imaging:

Immunofluorescence staining and microscopy have been described in detail before (11). Briefly, unaffected and affected fibroblasts were grown on cover slips a day before the experiment. For cellular mitochondrial visualization, the cells were incubated with a mitochondrial-specific dye MitoTracker Red CMXRos 580 (100 nM; Molecular Probe, Eugene, OR) for 30 min in the incubation chamber, washed, fixed in 4% paraformaldehyde, washed, counterstained with DAPI (4 ′-6-diamidino-2-phenylindole) during the washes, and mounted on a glass slide with Aqua Poly/Mount (Polysciences, Warrington, PA). Cells were observed with DeltaVision RT Deconvolution Microscope (Applied Precision, Issaquah, WA). The obtained images were deconvoluted to remove the reflective fluorescence using softWoRx software. Red and blue fluorescence were imaged with a confocal microscope with 63x objective lens. Slides were

imaged with a DeltaVision workstation (Applied Precision, Issaquah, WA). Z-stack images for red and blue fluorescence were acquired and were deconvolved using SoftWoRx (Applied Precision).

For immunofluorescence images of HeLa cells, cells were plated on a 8-well chamber slide (Ibidi, 80826), and fixed in formalin the next day. Slides were blocked with 10% goat serum in PBS-T (0.25% Triton X-100 in PBS) for 1 hour at room temperature, followed by probing with αTOMM40 antibody (Proteintech, 18409-1-AP) overnight at 4°C. Slides were washed in PBS-T, and then stained with AF594-conjugated αrabbit IgG (Invitrogen A11012) and DAPI for 1 hour at room temperature. Slides were mounted and imaged using a Zeiss LSM880 confocal microscope. GFP signals were obtained from its native fluorescence.

Reagents

Antibodies to the following proteins were used: TOMM7 (Invitrogen PA5-110508), TOMM20 (Proteintech 11802-1-AP), TOMM40 (Proteintech 18409-1-AP), TOMM22 (Proteintech (11278-1-AP), OXPHOS (including ATP5A, UQCRC2, SDHB, NDUFB8) (Abcam ab110413), ACTIN (Proteintech HRP-60008), TFAM (PA5-29571), HSP60 (Proteintech 15282-1-AP), AF594 goat αrabbit Igg (Invitrogen A11012), and FLAG (Proteintech 20543-1-AP). Oligomycin (Sigma 04876), CCCP (Sigma C2759), and antimycin A (Sigma A8674) were obtained from Sigma-Aldrich.

Constructs expressing wild-type and mutant (P29L) TOMM7 (with N-terminal FLAG, HA or GFP tags) were constructed by standard cloning and site-direct mutagenesis. HA-TOMM7 constructs were cloned into the lentiviral vector pKAM-ME-FLAG-BFP (Addgene, 101868). GFP-TOMM7 constructs were cloned into the lentiviral vector pLv (Addgene, 26808). YFP-Parkin cDNA was obtained from Addgene (plasmid 23955) and inserted into the lentiviral vector (pLv). Lentiviral plasmids were transfected along with helper plasmids psPAX2 and pMD2.G to create lentiviral particles in HEK293 cells.

Oxygen Consumption Rate (OCR) Measurements

Cells were plated at 10,000 cells per well (for human fibroblasts) or 15,000 cells per well (for mouse fibroblasts) in an XFe96 well plate (Seahorse Bioscience) in DMEM. The next day, three washes were performed with assay media (Sigma D5030, supplemented with 2mM L-glutamine, 10mM glucose, 100U/mL penicillin/streptomycin, pH 7.4), and incubated at 37°C in a non-CO2 incubator for 45 min. OCR was measured in a Seahorse XFe96 instrument using consecutive measurements, followed by 3 min mixing periods. Oligomycin (final concentration 2 µM), CCCP (final concentration 1 µM), and antimycin A (final concentration 2 µM) were sequentially injected to assess basal, maximal and non-mitochondrial OCR. Basal (pre-injection) and maximal (post-CCCP injection) OCR was calculated by subtracting antimycin-inhibited OCR, followed by normalization for number of cells. A linear mixed model (GraphPad Prism) was used to test differences between proband and control human fibroblasts, or wild-type and *Tomm7*$^{P29L/P29L}$ mouse fibroblasts.

Mitophagy experiments

Patient-derived fibroblast lines were transduced with YFP-Parkin expressing lentivirus; 48 hours later, cells were treated with fresh media containing either DMSO or CCCP (10 µM). Cells were fixed and stained for Tomm20 and nuclei (DAPI) at 3 hr and 24 hr post media exchange, and imaged on a Zeiss LSM880 confocal microscope.

Mitochondrial isolation

Mitochondria were purified from patient and four control fibroblast cell lines for proteomic analysis. Cells were trypsinized from 10 cm plates of fibroblasts, followed by mitochondrial isolation using previously published protocols.(12) Briefly, cells were washed in isolation buffer (5

mM HEPES, 220 mM mannitol, 70 mM sucrose, 70 mM KCl, .5 mM EGTA, 10 mM KH_2PO_4, 5mM $MgCl_2$, supplemented with protease inhibitors), and lysed via dounce homogenization. Lysates were cleared of cell debris with four 600xg spins. A crude mitochondrial fraction was isolated from the lysate using a 10000xg spin, followed by three washes in isolation buffer. Mitochondrial pellets were solubilized in 1 x RIPA buffer.

Proteomics Experiments

Label-free quantitative proteomics was performed in lysates from human or mouse fibroblasts as follows: 50 µg of protein was loaded onto a 4-20% Mini-PROTEAN TGX precast protein gel (BioRad), stained with Coomassie Blue, and destained. After excision from gel, samples were digested overnight with trypsin (Pierce) following by reduction and alkylation with DTT and iodoacetamide (Sigma–Aldrich), solid-phase extraction cleanup with an Oasis HLB plate (Waters) and injection onto an Orbitrap Fusion Lumos mass spectrometer coupled to an Ultimate 3000 RSLC-Nano liquid chromatography system. Samples were injected onto a 75 µm i.d., 75-cm long EasySpray column (Thermo) and eluted with a gradient from 0-28% buffer B over 90 min. Buffer A contained 2% (v/v) ACN and 0.1% formic acid in water, and buffer B contained 80% (v/v) ACN, 10% (v/v) trifluoroethanol, and 0.1% formic acid in water. The mass spectrometer operated in positive ion mode with a source voltage of 1.8 kV and an ion transfer tube temperature of 275 °C. MS scans were acquired at 120,000 resolution in the Orbitrap and up to 10 MS/MS spectra were obtained in the ion trap for each full spectrum acquired using higher-energy collisional dissociation (HCD) for ions with charges 2-7. Dynamic exclusion was set for 25 s after an ion was selected for fragmentation. Raw MS data files were analyzed using Proteome Discoverer v2.4 SP1 (Thermo), with peptide identification performed using Sequest HT searching against the human protein database from UniProt. Fragment and precursor tolerances of 10 ppm and 0.6 Da were specified, and three missed cleavages were allowed. Carbamidomethylation of Cys was set

as a fixed modification, with oxidation of Met set as a variable modification. The false-discovery rate (FDR) cutoff was 1% for all peptides. After normalization by total ion count, proteins were filtered for presence in MitoCarta 3.0. Protein abundance of each sample was normalized by the total ion counts. Each of the 5 cell lines were measured 3 to 6 times. For each cell line, only proteins detected in all replicates were considered and mean was used as the final measurement of a protein. Differential protein expression analysis was performed using DEqMS (v1.14) (13). Proteins were further filtered for presence in MitoCarta 3.0 (14). Gene set enrichment analysis was performed using WebGestalt 2019 (15). Enriched pathways with false discovery rate (FDR) less than 0.05 were reported. For analysis of mitochondrial ETC proteins, a custom gene set was used (Table S1).

Immunoprecipitation experiments:

HEK293 cells were transfected with FLAG-TOMM7^{wt}, FLAG-TOMM7^{P29L} or GFP expressing plasmids. Cells were collected and washed with ice cold PBS 48hr after transfection, and lysed with Pirece IP lysis Buffer (PI 87787) according to manufacturer instructions. 120 µl of these supernatants were reserved as control inputs. The remaining supernatants were transferred into 1.5 mL microcentrifuge tubes containing prewashed Anti-Flag Magnetic Beads (Sigma M8823) and incubated at 4℃ overnight with mixing. The beads were washed three times with ice cold TBS-T (25mM Tris/HCl pH7.6, 150mM NaCl, 0.1% (v/v) Tween 20) and then re-suspended in 120 µL TBS containing 25µg/µL 3X Flag peptide. After 30 min incubation at 4℃ with gentle shaking, the beads were removed via magnet, and the eluate collected. Immunoprecipitation experiments in *Tomm7*$^{-/-}$ HeLa cells were performed using the Pierce αHA magnetic beads (Thermo Fisher 88836) following manufacturing instructions. Briefly, cell lysates (prepared as above) were incubated with 25 µL of αHA magnetic beads (pre-washed with TBS + 0.05% Tween20) in 1.5mL

microcentrifuge tubes for 30 minutes at room temperature. Beads were collected and washed using a magnetic stand, and then boiled in SDS-PAGE sample buffer (BioRad, 1610747).

Statistical Methods:

No statistical tests were used to predetermine sample size, and no data were excluded. For statistical assessment of proteomics datasets, DeqMS was utilized. Gene set enrichment analysis was performed using WebGestalt 2019. Enriched pathways with false discovery rate (FDR) less than 0.05 were reported. A linear mixed model (GraphPad Prism) was fit to test the differences in oxygen consumption rate (OCR) between the proband and control fibroblasts and between wild-type and *Tomm7*$^{P29L/P29L}$ mouse fibroblasts. For representative imaging data from cell lines, the experiment was conducted at least three times. For human clinical assessment and imaging, data was collected once unless otherwise indicated. Percentiles of height and body weight across ages were based on values from the Centers for Disease Control.

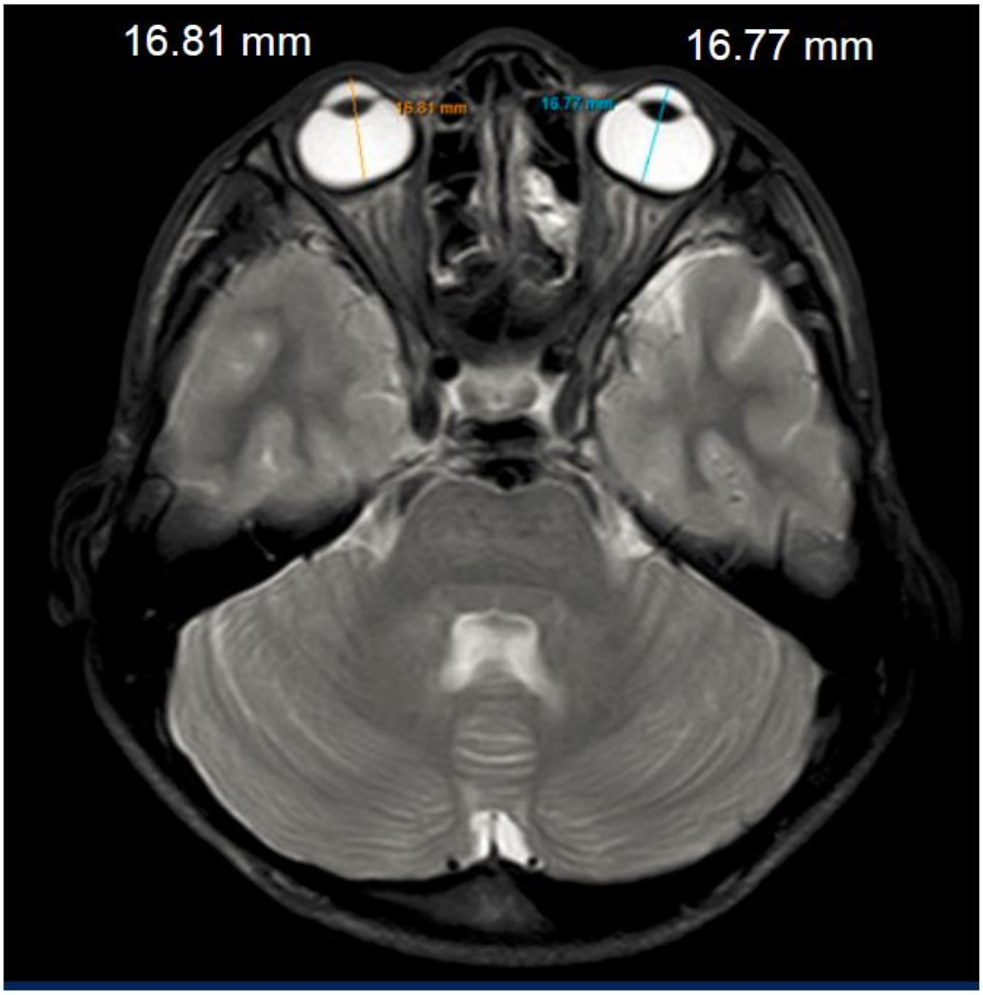

Supplementary Figure S1. Axial Magnetic Resonance Image of the proband's head at the level of the eyeballs. The length of the orbit was 16.81 mm on the right side and 16.77 mm on the left side revealing micro-ophthalmia. Normal axial length is between 22-25 mm (16).

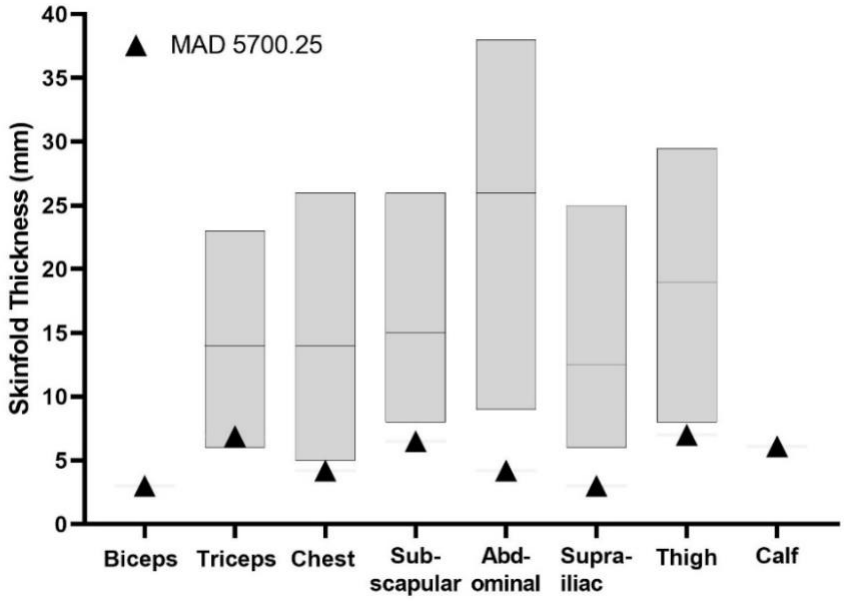

Supplementary Figure S2. Skinfold thickness of the proband at various anatomical sites of the body compared to normal data. Skinfold thickness data of MAD 5700.25 at 19 years of age are shown as triangles. The gray vertical bars indicate 10th to 90th percentile values of normal males with median value as horizontal line in between the bars (17).

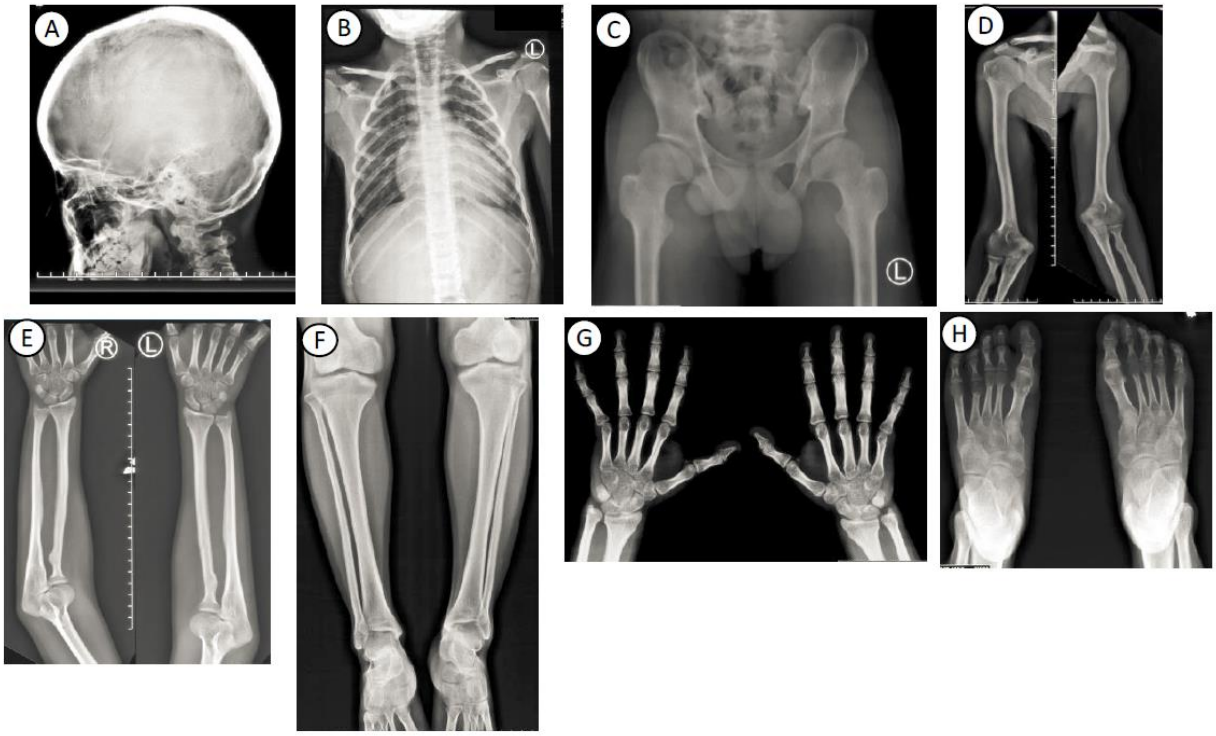

Supplemental Figure S3.

Radiologic skeletal survey of the patient at age 19 years. A. Skull X-ray lateral view shows normal cranial vault with proportionate midfacial bones. The mandible was small with obtuse mandibular angle. No Wormian bones were visualized. B. Chest X-ray shows elongated rib cage and splaying of the costochondral junctions bilaterally. Heart is slightly enlarged. Clavicles and scapulae are normal. C. X-ray of pelvis reveals small and shallow pelvis with small iliac wings. Acetabular fossae are shallow. Femoral heads are widened and flat and prominent. D & E. X-ray of the arms and forearms show bilateral humeri, radii/ulnae are symmetrical and proportionately small. The head and medial and lateral epicondyles of the humeri are disproportionately prominent and there is a cubitus valgus deformity bilaterally. Bilateral periarticular osteopenia is present around the elbow joints. F. X-ray of the legs show slight prominence of medial femoral condyles. G. Periarticular osteopenia around the joints of the hands. All the epiphyses of the hand are fused. No osteolysis is observed. H. X-ray of the feet shows bilateral periarticular regional osteopenia involving the head of all metatarsal bones, head and bases of all phalanges. There is shortening

of the left 4th metatarsal bone. Estimated bone age is consistent with the chronologic age. Thoraco-lumbar and lumbo-sacral spine X-rays showed loss of thoracic kyphosis and lumbar lordosis. Vertebral body heights and intervertebral discs were preserved (no images shown).

.

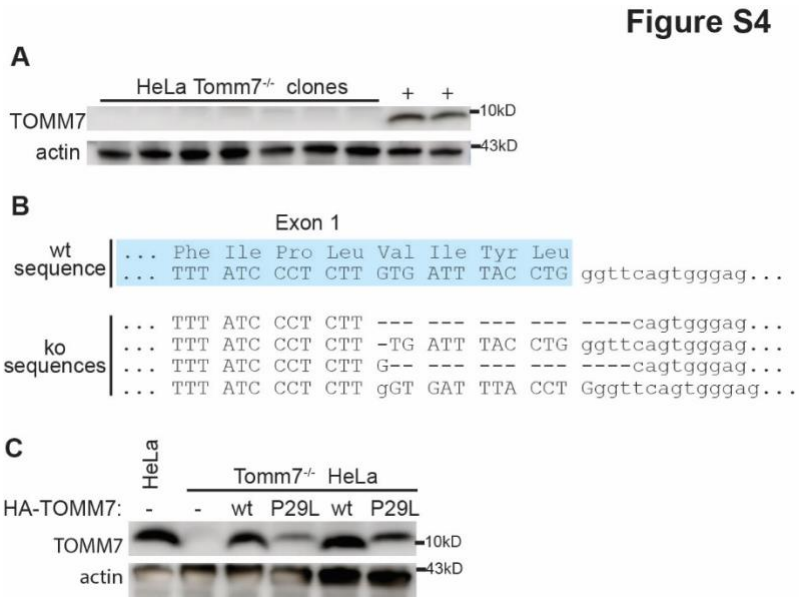

Supplemental Figure S4. Generation of *Tomm7*$^{-/-}$ HeLa cell lines. A. TOMM7 levels assessed by western blot of individual clones from transfection of HeLa cells with sgRNA-containing plasmids targeting exon1 of Tomm7. Wild-type clones are indicated by '+'. Actin levels are shown as a loading control. B. Genome sequencing of individual alleles from a *Tomm7*$^{-/-}$ HeLa cell line. The wild-type sequence is shown for reference, and individual knockout allele sequences are provided. C. Western blot of *Tomm7*$^{-/-}$ cells reconstituted with wild-type or P29L variants of HA-TOMM7, via lentivirus transduction. Actin levels are shown as a loading control.

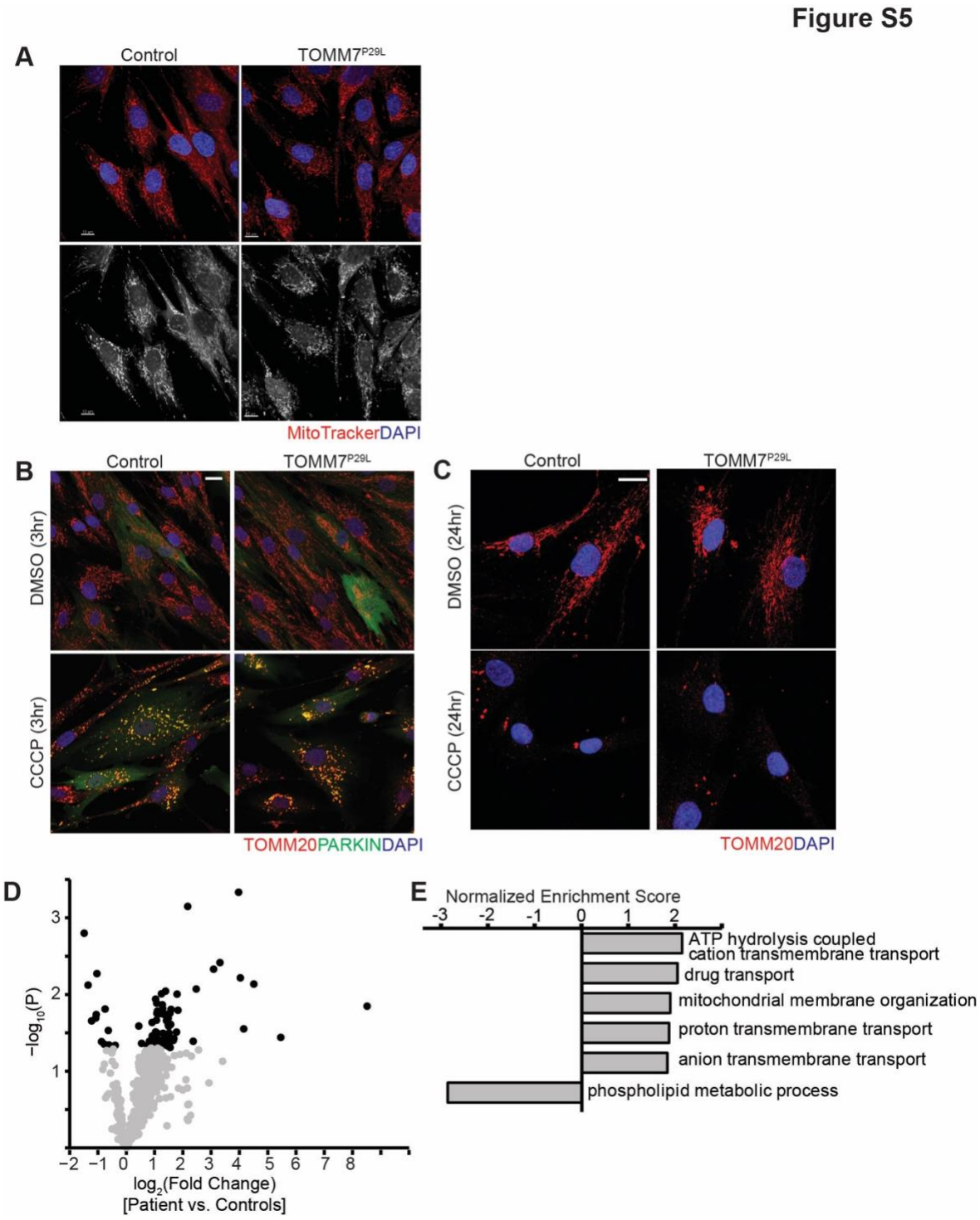

Supplementary Figure S5. Mitochondrial properties in MAD5700.25 fibroblasts.

A. Mitochondrial morphology was assessed in proband and control fibroblasts. Representative merged images for mitochondria (MitoTracker Red; red) and nuclei (DAPI, blue). The same

images are also shown on the right, except that the false coloring has been removed. B. Parkin recruitment is not impaired in proband (TOMM7$^{P29L)}$ fibroblasts. Parkin (green) translocation to mitochondria in response to dimethyl sulphoxide (DMSO) or carbonyl cyanide m-chlorophenylhydrazone (CCCP) (3 hours) in control and patient fibroblast cell lines. Mitochondria are visualized with anti-TOMM20 staining (red), and nuclei are stained with 4′,6-diamidino-2-phenylindole (DAPI; blue). C. Mitophagy is not impaired in proband (TOMM7^{P29L}) fibroblasts. Mitochondria are visualized by anti-TOMM20 staining (red), and are largely cleared 24 hours post-CCCP treatment in both control and TOMM7^{P29L} fibroblasts. Nuclei are stained by DAPI (blue). D. Volcano plot of differentially expressed proteins from the proband's mitochondria vs. controls. Differentially expressed proteins at a p-value less than 0.05 are displayed in black. E. Gene set enrichment analysis of mitochondrial proteins in proband vs. control fibroblasts. Gene sets with false discovery rate < 0.05 are shown. A positive or negative normalized enrichment score indicates enrichment of up- or down-regulated genes in the pathway, respectively.

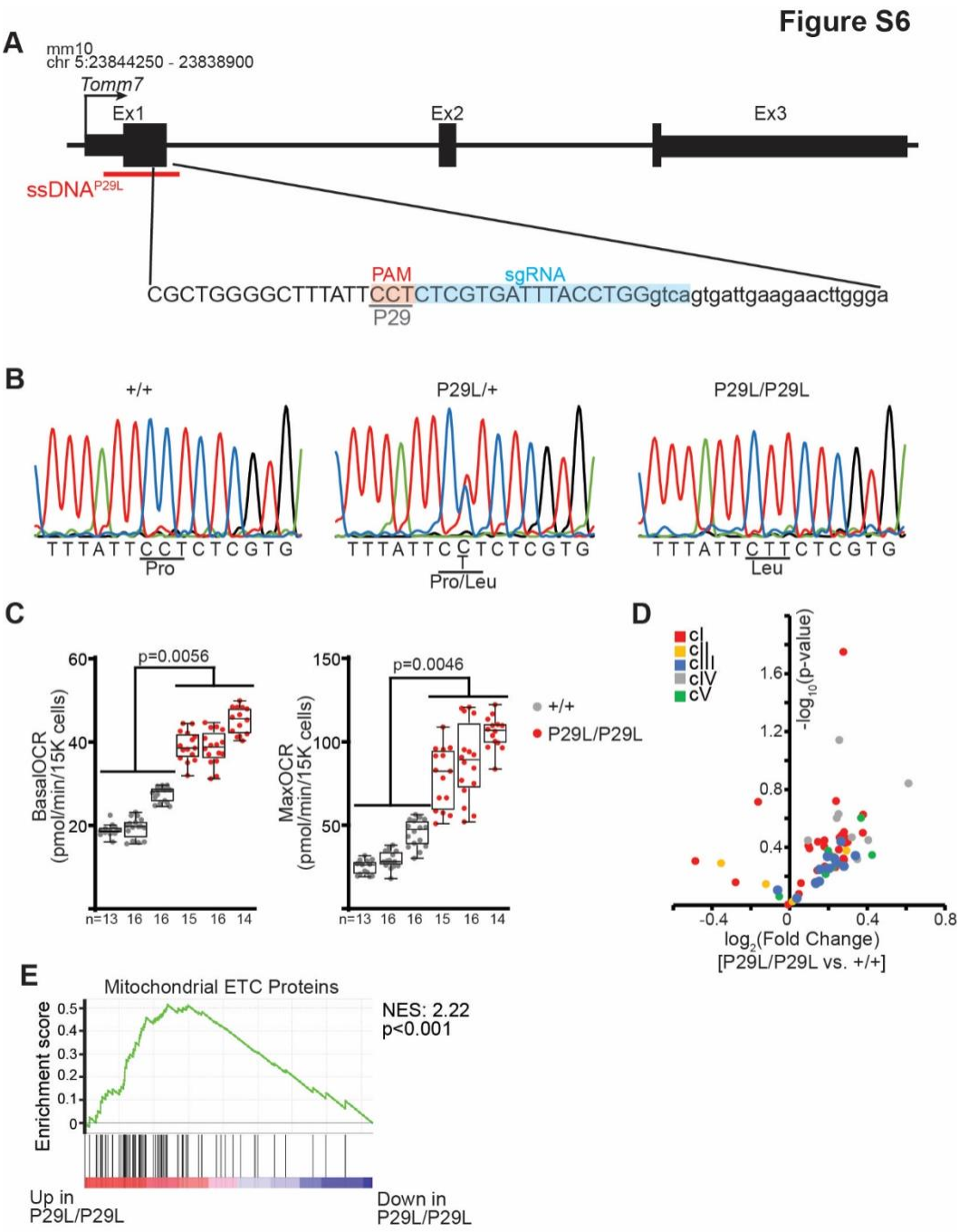

Supplementary Figure S6. Analysis of *Tomm7*$^{P29L/P29L}$ mouse neonatal tail fibroblasts. A. Schematic of CRISPR-targeting strategy for editing of the endogenous mouse Tomm7 locus. A sgRNA targeting the blue-highlighted sequence was synthesized to target Cas9 to the locus; the PAM motif is shown in red, and overlaps the Proline 29 position. The position of the single-stranded DNA (ssDNA) species (335bp) spanning this region and containing the P29L mutation

is shown in red. B. Sanger sequencing of the mouse *Tomm7* locus surrounding Proline29 from tail DNA of engineered animals. Wild-type (+/+), heterozygous (P29L/+), and homozygous (P29L/P29L) sequencing is shown. C. Increased basal and maximal (uncoupled) oxygen consumption rates (OCR) measured in P29L/P29L versus wild-type (+/+) fibroblast cell lines. Each independent fibroblast cell line was measured >13 times, and a linear mixed model (GraphPad Prism) was fit to test the difference between P29L/P29L and +/+ cell lines**.** D. Volcano plot of mitochondrial ETC component protein abundance in P29L/P29L versus +/+ cell lines. Individual proteins are color-coded based on the mitochondrial complex with which they are associated. E. Gene set enrichment analysis of mitochondrial ETC components in P29L/P29L versus +/+ cell lines. The normalized enrichment score (NES) and p-value are indicated.

References:

1. McKenna A, Hanna M, Banks E, Sivachenko A, Cibulskis K, Kernytsky A, Garimella K, Altshuler D, Gabriel S, Daly M, et al. The Genome Analysis Toolkit: a MapReduce framework for analyzing next-generation DNA sequencing data. *Genome Res.* 2010;20(9):1297-303.
2. Cingolani P, Platts A, Wang le L, Coon M, Nguyen T, Wang L, Land SJ, Lu X, and Ruden DM. A program for annotating and predicting the effects of single nucleotide polymorphisms, SnpEff: SNPs in the genome of Drosophila melanogaster strain w1118; iso-2; iso-3. *Fly (Austin).* 2012;6(2):80-92.
3. Davydov EV, Goode DL, Sirota M, Cooper GM, Sidow A, and Batzoglou S. Identifying a high fraction of the human genome to be under selective constraint using GERP++. *PLoS Comput Biol.* 2010;6(12):e1001025.
4. Kircher M, Witten DM, Jain P, O'Roak BJ, Cooper GM, and Shendure J. A general framework for estimating the relative pathogenicity of human genetic variants. *Nature Genetics.* 2014;46(3):310-5.
5. Narasimhan V, Danecek P, Scally A, Xue Y, Tyler-Smith C, and Durbin R. BCFtools/RoH: a hidden Markov model approach for detecting autozygosity from next-generation sequencing data. *Bioinformatics.* 2016;32(11):1749-51.
6. Talevich E, Shain AH, Botton T, and Bastian BC. CNVkit: Genome-wide copy number detection and visualization from targeted DNA sequencing. *PLoS Comput Biol.* 2016;12(4):e1004873.
7. Chen X, Schulz-Trieglaff O, Shaw R, Barnes B, Schlesinger F, Kallberg M, Cox AJ, Kruglyak S, and Saunders CT. Manta: rapid detection of structural variants and indels for germline and cancer sequencing applications. *Bioinformatics.* 2016;32(8):1220-2.
8. Khan M, and Gasser S. Generating primary fibroblast cultures from mouse ear and tail tissues. *Journal of visualized experiments:* 2016; (107):e53565.
9. Sankella S, Garg A, and Agarwal AK. Activation of sphingolipid pathway in the livers of lipodystrophic *Agpat2*(-/-) Mice. *J Endocr Soc.* 2017;1(7):980-93.
10. Agarwal AK, Arioglu E, De Almeida S, Akkoc N, Taylor SI, Bowcock AM, Barnes RI, and Garg A. AGPAT2 is mutated in congenital generalized lipodystrophy linked to chromosome 9q34. *Nature Genetics.* 2002;31(1):21-3.
11. Prasad SS, Garg A, and Agarwal AK. Enzymatic activities of the human AGPAT isoform 3 and isoform 5: localization of AGPAT5 to mitochondria. *J Lipid Res.* 2011;52(3):451-62.
12. Mishra P, Carelli V, Manfredi G, and Chan DC. Proteolytic cleavage of Opa1 stimulates mitochondrial inner membrane fusion and couples fusion to oxidative phosphorylation. *Cell Metab.* 2014;19(4):630-41.
13. Zhu Y, Orre LM, Zhou Tran Y, Mermelekas G, Johansson HJ, Malyutina A, Anders S, and Lehtio J. DEqMS: A method for accurate variance estimation in differential protein expression analysis. *Mol Cell Proteomics.* 2020;19(6):1047-57.
14. Rath S, Sharma R, Gupta R, Ast T, Chan C, Durham TJ, Goodman RP, Grabarek Z, Haas ME, Hung WHW, et al. MitoCarta3.0: an updated mitochondrial proteome now with sub-organelle localization and pathway annotations. *Nucleic Acids Res.* 2021;49(D1):D1541-D7.
15. Liao Y, Wang J, Jaehnig EJ, Shi Z, and Zhang B. WebGestalt 2019: gene set analysis toolkit with revamped UIs and APIs. *Nucleic Acids Res.* 2019;47(W1):W199-W205.
16. Dong J, Zhang Y, Zhang H, Jia Z, Zhang S, and Wang X. Comparison of axial length, anterior chamber depth and intraocular lens power between IOLMaster and ultrasound in normal, long and short eyes. *PLoS One.* 2018;13(3):e0194273.
17. Jackson AS, and Pollock ML. Generalized equations for predicting body density of men. *British Journal of Nutrition.* 1978;40(3):497-504